Bull Volcanol (2012) 74:1395–1407
DOI 10.1007/s00445-012-0598-9

RESEARCH ARTICLE

# Monitoring of the plume from the basaltic phreatomagmatic 2004 Grímsvötn eruption—application of weather radar and comparison with plume models

**Björn Oddsson · Magnús T. Gudmundsson · Guðrún Larsen · Sigrún Karlsdóttir**

Received: 12 February 2011 / Accepted: 25 March 2012 / Published online: 29 April 2012


**Abstract** The Grímsvötn eruption in November 2004 belongs to a class of small- to medium-sized phreatomagmatic eruptions which are common in Iceland. The eruption lasted 6 days, but the main phase, producing most of the 0.02 km$^3$ of magma erupted, was visible for 33 h on the C-band weather radar of the Icelandic Meteorological Office located in Keflavík, 260 km to the west of the volcano. The plume rose to 8–12 km high over sea level during 33 h. The long distance between radar and source severely reduces the accuracy of the plume height determinations, causing 3.5-km steps in recorded heights. Moreover, an apparent height overestimate of ~1.5 km in the uncorrected radar records occurs, possibly caused by wave ducting or super-refraction in the atmosphere. The stepping and the height overestimate can be partly overcome by averaging the plume heights and by applying a height adjustment based on direct aircraft measurements. Adjusted weather radar data on plume height are used to estimate the total mass erupted using empirical plume models mostly based on magmatic eruptions and to compare it with detailed in situ measurements of the mass of erupted tephra. The errors arising because of the large radar plume distance limit the applicability of the data for detailed comparisons. However, the results indicate that the models overestimate the mass erupted by a factor of three to four. This supports theoretical models indicating that high steam content of phreatomagmatic (wet) plumes enhances their height compared to dry plumes.

**Keywords** Explosive eruptions · Magma discharge · Plume models · Iceland

Editorial responsibility: J.C. Phillips

B. Oddsson (✉) · M. T. Gudmundsson · G. Larsen
Institute of Earth Sciences, University of Iceland,
Sturlugata 7,
IS-101 Reykjavík, Iceland
e-mail: bjornod@hi.is

S. Karlsdóttir
Icelandic Meteorological Office,
Bústaðavegur 9,
150 Reykjavík, Iceland

## Introduction

Volcanic eruption plumes carry tephra and volcanic gasses into the atmosphere and may transport these products to great distances from the source volcano. At distal locations, the solid particles of the plume are mostly ash or fine ash (e.g., Rose and Durant 2009) and the reach and severity of the fallout is of major concern for volcanic hazard, both to local populations and regional and sometimes global air traffic, as exemplified by the Eyjafjallajökull eruption in April–May 2010 (Gudmundsson et al. 2010). Estimates of flux of magma during explosive eruptions are very approximate, and the only method that can be used in real time is the application of empirical or theoretical formulas relating plume height and magma discharge (Wilson et al. 1978; Sparks 1986; Sparks et al 1997; Carey and Bursik; 2000; Mastin et al. 2009). Thus, during explosive volcanic eruptions, accurate definition of plume height at any given time is of major importance for hazard assessment, not least for prediction of ash concentration and transport in the atmosphere by Volcanic Ash Advisory Centres (VAACs). Various types of weather radars have been used for determination of plume height and eruption magnitude (e.g., Rose et al. 1995; Lacasse et al. 2004; Vogfjörd et al. 2005; Scollo et al. 2009; Webley and Mastin 2009; Marzano et al. 2010).

At the time of the 2004 eruption, a single C-band weather radar operated by the Icelandic Meteorological Office (IMO) existed in Iceland, located close to Keflavík Airport, near the

south westernmost tip of the island (Fig. 1). The most active volcanoes are located in the Eastern and Northern Volcanic Zones, 100–300 km distant from the radar. These large distances limit the use of the weather radar to detect ash from more distant volcanoes, including the highly active Grímsvötn, 260 km to the east-northeast of the radar station. The eruption of Grímsvötn on November 1–6, 2004 was monitored with the radar as well as through repeated aerial observations that included plume height determination by aircraft. The eruption produced a well-defined fan of tephra during the 33-h long main phase of activity. The fan extended towards north and northeast over the Vatnajökull glacier where most of the tephra was deposited (Oddsson 2007). Deposition onto a glacier in winter, securing full preservation until the following summer, allowed detailed and accurate mapping of fall deposit mass. Hence, a reliable estimate of fall deposit mass could be made and combined with plume height records; the eruption provides a test for plume height–magma discharge models for a basaltic phreatomagmatic eruption. The aims of the present paper are (1) to explore the usefulness and limitations of volcanic plume height determination by distant weather radar and (2) to compare plume heights and magma discharge records of this basaltic phreatomagmatic eruption with magma discharge models.

## Field setting

The Grímsvötn central volcano is about 15 km in diameter and located in the centre of the 8,100 km$^2$ Vatnajökull ice cap in Southeast Iceland (Fig. 1). It is mostly overlain by 300–700 m thick ice (Björnsson 1988), and apart from a few nunataks and the southern caldera wall, it is completely ice covered. It hosts one of the most powerful geothermal areas in the world (Björnsson et al. 1982; Björnsson and Guðmundsson 1993), and within its south caldera is a sub-glacial lake, covered by about 250 m thick ice shelf. Grímsvötn has higher eruption frequency than any other Icelandic volcano, with eruptions occurring about once every 5–10 years during 60–80-year long episodes of elevated activity, which alternate with episodes of similar duration when eruptions are much less frequent (Larsen et al. 1998). A cycle of high activity is considered to have began in 1996, with the flank eruption in Gjálp and eruptions in the Grímsvötn caldera in 1998, 2004 (Gudmundsson et al. 2004; Gudmundsson 2005; Thordarson and Larsen 2007) and the most recent one in May 2011.

Most Grímsvötn eruptions occur on short fissures just within and trending parallel with the southern caldera fault. These eruptions usually melt or force their way through 50–200 m of ice in a few minutes to an hour (Gudmundsson and Björnsson 1991; Gudmundsson 2005; Jakobsson and Gudmundsson 2008). The eruptive products have, in the last several hundred years, been basalt (Larsen et al. 1998). Since the eruptions occur through water and ice, they are phreatomagmatic. Most Grímsvötn eruptions within the caldera are small (volume <0.1 km$^3$, dense rock equivalent, DRE), and fallout of tephra is usually confined to Vatnajökull and neighbouring areas. However, this is not without exception, since records indicate that ash from the eruption in 1619 was detected in Scandinavia (Thorarinsson 1980), and the most recent eruption in May 2011 carried minor amounts of ash to the British Isles (Stevenson et al. 2012). Eruptions usually last a few days to a few weeks (Thorarinsson 1974; Gudmundsson 2005). Fissure eruptions outside the caldera are much less frequent and appear to be an order of magnitude larger, e.g., the eruptions in Gjálp in 1938 and 1996 (Gudmundsson and Björnsson 1991; Gudmundsson et al. 2004).

## The Grímsvötn eruption in 2004

This eruption is described in detail elsewhere (Sigmundsson and Guðmundsson 2004; Vogfjörd et al. 2005; Oddsson 2007 and Jude-Eton et al. 2012) and therefore only a necessary outline is presented here. Seismicity was elevated for several months preceding the eruption on 2004, with escalation in seismic unrest in the second half of October 2004, and an intense swarm of earthquakes before the outbreak at about 21:50 UTC on 1 November (Vogfjörd et al. 2005). The eruption is considered to have been triggered by pressure release when the water level of the subglacial lake dropped as it was drained in a jökulhlaup that started on October 28 (Albino et al. 2010). Darkness and poor weather conditions prevented visual observations until on the morning of November 2, but on a weather radar, a plume was detected at 23:00 UTC November 1, which rose for the next 3 h reaching an apparent height close to 14 km above sea level (an overestimate—see below). The explosive eruption continued with similar magnitude until 8:30 UTC on November 3. A reconstruction of the activity based on proximal deposit stratigraphy and correlation with seismic tremor records has been presented by Jude-Eton et al. (2012). It suggests that the fully subglacial phase may have lasted only 23 min and that plume transport dropped substantially after 9:58 UTC on November 3, while some local deposition amounting to a few tens of cubic meter per second DRE continued from a low plume until late afternoon on that same day. After November 3, activity was minor, with observations of mild explosive activity in the following days with the plume only rising 1–2 km over the vent (Oddsson 2007). On November 6, when weather conditions did not allow visual observations, the seismic tremor dropped to background levels, and the eruption is considered to have terminated. This was confirmed in an inspection flight on November 7.

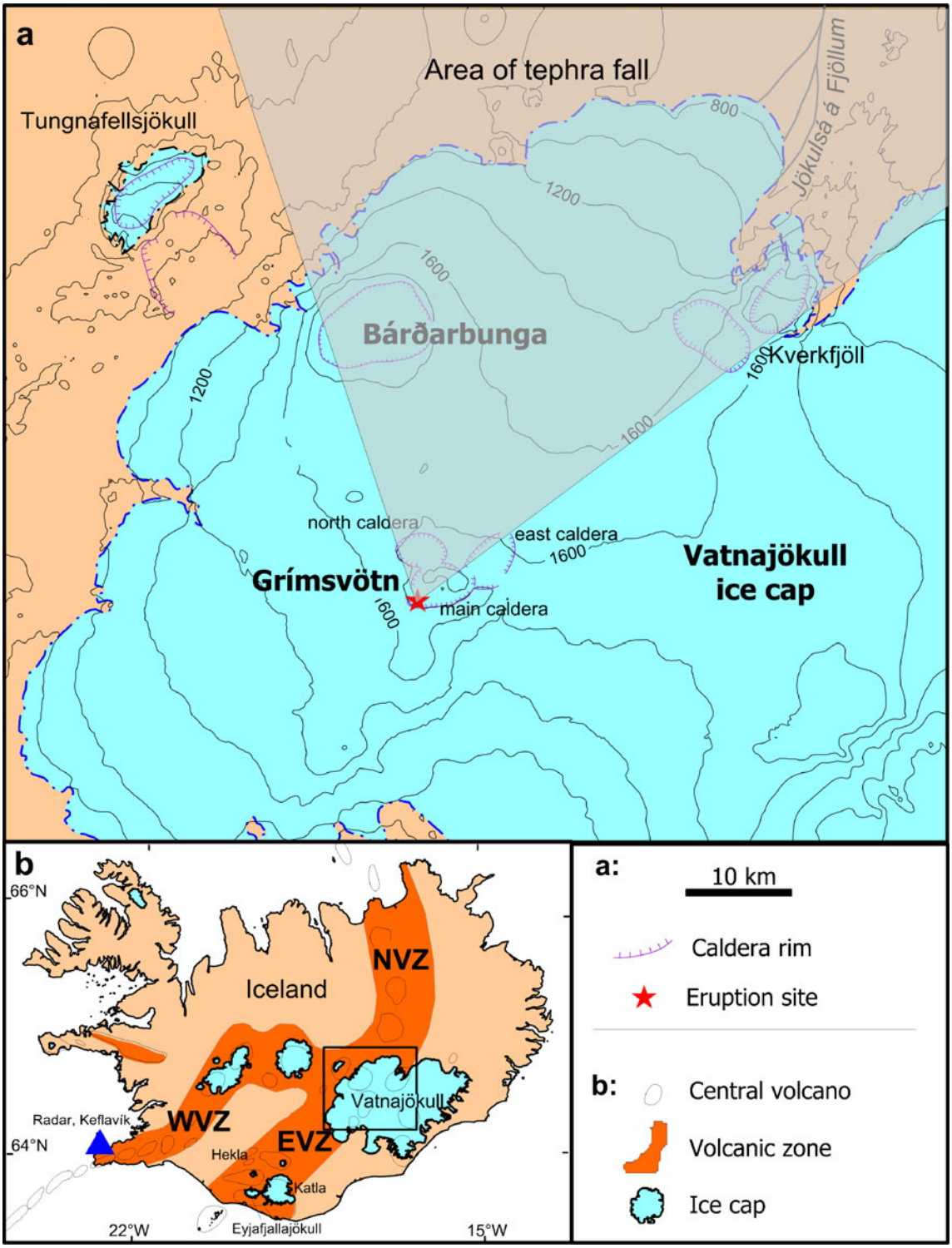


**Fig. 1** Geographical setting of Grímsvötn, Vatnajökull and the tephra fans formed in the eruption at Grímvötn in 2004. **a** The northwest part of Vatnajökull with Grímsvötn and the 2004 eruption site in the southwest corner of the caldera. The tephra fall during the main phase of the eruption on November 2–3 occurred within a sector between the north-northwest and northeast. **b** The main volcanic zones and central volcanoes in Iceland. *EVZ* Eastern Volcanic Zone, *WVZ* Western Volcanic Zone, *NVZ* Northern Volcanic Zone. Based on Saemundsson (1979)

The eruption produced in total $5.6\pm1.0\times10^{10}$ kg of basaltic phreatomagmatic tephra with an average in situ (bulk) density of 1,190±40 kg m$^{-3}$ (Oddsson 2007), corresponding to a bulk volume of $47\pm8\times10^{6}$ m$^3$ or $20\pm4\times10^{6}$ m$^3$ DRE. The total

amount of eruptive material was measured in the summers of 2005 and 2006. The tephra layer was very well preserved in the accumulation area of Vatnajökull glacier, since it was covered by winter snow during and immediately after the eruption. This prevented any post-eruption re-deposition of the tephra. In the proximal area where the layer was thickest, direct measurements of thickness were made and the bulk density measured. Elsewhere on the glacier, a core through the snow containing the tephra layer was obtained with a snow corer. The mass of tephra in the core was measured, providing a value of mass per unit area. To the north of the glacier, the tephra was sampled in the days immediately after the eruption and, as was done on the glacier, the mass per unit area was obtained. An isomass map of the tephra deposit was drawn and digitised (Fig. 2). The most reliable estimate of the mass of the tephra layer outside the vent area is obtained by integrating this map, with the error margins considered to be 15–20 % (Oddsson 2007).

Almost half of the erupted material, $2.8\pm0.5\times10^{10}$ kg, was deposited as tephra in a 750 m long, 550 m wide and 150–200 m deep ice cauldron that the eruption melted in the glacier in the first one and a half days around the volcanic vents (Oddsson 2007; Jude-Eton et al. 2012). The remaining $2.7\pm0.5\times10^{10}$ kg fell as proximal and distal tephra outside the ice cauldron. About 95 % of the total mass was erupted during the main 33-h long phase of activity, after the brief initial subglacial phase, i.e., between 22:17 UTC on November 1 and 10:00 UTC on November 3 (Jude-Eton et al. 2012). The volcanic material outside the cauldron was, over this period, deposited in two, partly overlapping and well-defined sectors to the north and northeast of the volcano.

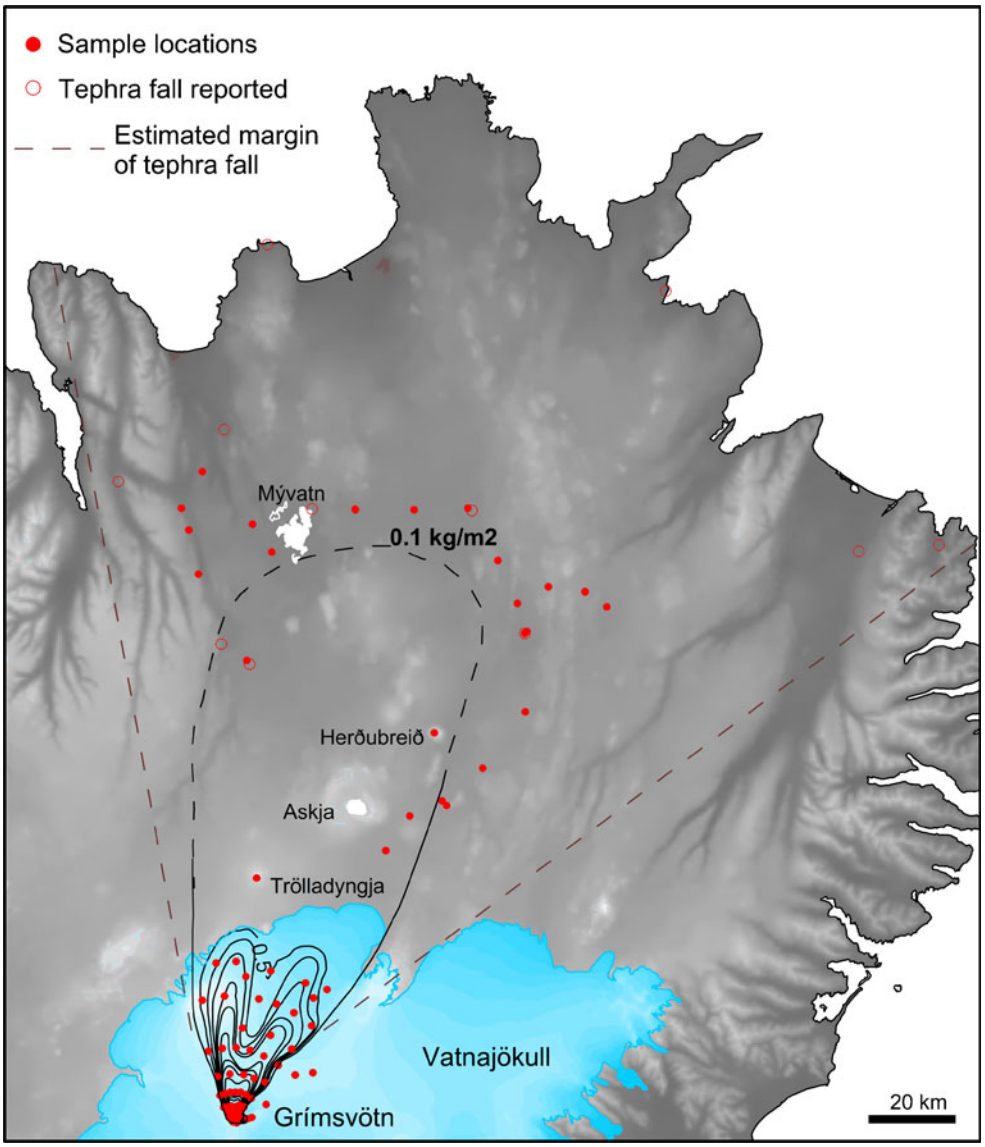


**Fig. 2** Distribution of the 2004 Grímsvötn tephra and localities where tephra was detected or measured, presented as isomass lines. The outermost isomass line is 0.1 kg/m$^2$ (equivalent to 0.1 mm thickness) and reached Mývatn about 140 km to the north of the eruption site. Minor tephra fall was reported at several locations on the north coast

## Eruption column models

### Theoretical approach to the top height of volcanic plumes

It has been shown that eruption column height is a nonlinear function of the mass erupted and atmospheric stratification. Morton et al. (1956) proposed an equation to express the relationship between the input rate of thermal energy to the plume and the top height of a maintained plume from a steady source (fires, smokestacks or burning forests):

$$H = 31(1+n)^{-3/8}\dot{Q}^{1/4}, \tag{1}$$

where $H$ is the height (meter), $\dot{Q}$ is the rate of production of thermal energy at source (kilowatt) and $n$ is the ratio of the vertical gradient of the absolute temperature to the lapse rate.

For an environmental lapse rate in a standard atmosphere of 6.5°C/km and an adiabatic lapse rate of 9.8°C/km (Wilson et al. 1978), Eq. 1 may be expressed as:

$$H = 31\left(1+\frac{6.5}{-9.8}\right)^{-3/8}\left(\frac{\dot{Q}}{1,000}\right)^{1/4} = 8.2\dot{Q}^{1/4}, \tag{2}$$

where the steady rate of release of thermal energy $\dot{Q}$ is:

$$\dot{Q} = \rho_m C_{p,m}(T_i - T_a)F\dot{Q}_V. \tag{3}$$

Here $C_{p,m}$ is the specific heat of the erupted material, $T_i$ is the initial temperature, $T_a$ is the final temperature of the material, $F$ is thermal efficiency and $\dot{Q}_V$ is the volume disharge rate (cubic meter per second) of magma with bulk density $\rho_m$. Combining Eqs. 2 and 3 gives Eq. 4, which relates the volume discharge rate ($\dot{Q}_V$) and maximum height of the plume ($H$):

$$H = 8.2\left(\rho_m C_{p,m}(T_i - T_a)F\right)^{1/4}\dot{Q}_V^{1/4} \tag{4}$$

We use commmon values for basaltic magmas given by McBirney (1993) $\rho_m$=2,600 kg m$^{-3}$, $C_p$ 1,100 Jkg$^{-1}$ °C$^{-1}$, $T_i$=1,150°C and $T_a$=0°C. By using $F$=0.7 from Sparks and Wilson (1976), the relationship between $\dot{Q}_V$ in cubic meter per second, and $H$ in kilometre is:

$$H = 1.85\,\dot{Q}_V^{1/4} \tag{5}$$

The model expressed in Eqs. 1–5 has been widely used for eruption columns which produce strong plumes (Settle 1978; Wilson et al. 1978; Sparks 1986).

### Empirical approach to the plume height

The simple plume theory of Morton et al. (1956) was verified by Wilson et al. (1978) and Settle (1978) by comparing a dataset of historical eruptions with information on the duration of a sustained period of explosive activity, eruption column height, total volume of ejecta and magma discharge rate. Two similar fully empirically-derived power law models have been presented using available plume height and eruption ejecta volume (Eq. 6: Sparks et al. 1997; Eq. 7: Mastin et al. 2009):

$$H = 1.67\,\dot{Q}_V^{0.259}, \tag{6}$$

$$H = 2.00\,\dot{Q}_V^{0.241}, \tag{7}$$

Here $H$ is the height in kilometre and $\dot{Q}_V$ is the DRE discharge rate of magma in cubic meter per second. The inverse forms of Eqs. 5–7 provide an estimate of magma discharge rate in an explosive eruption from the plume heights:

$$\text{Wilson et al. (1978)} : \dot{Q}_V = 0.085H^4 \tag{8}$$

$$\text{Sparks et al. (1997)} : \dot{Q}_V = 0.138H^{3.86} \tag{9}$$

$$\text{Mastin et al. (2009)} : \dot{Q}_V = 0.056H^{4.15} \tag{10}$$

Equation (9) has been used for estimating magma discharge rate in Icelandic eruptions (e.g., Gudmundsson et al. 2004; Lacasse et al. 2004; Höskuldsson et al. 2007). Below, all three models will be compared with actual magma discharge in Grímsvötn based on measured quantity of erupted material and duration of eruption.

## Weather radar

Ground-based weather radar has been used to detect volcanic plumes and measure height, location and other physical characteristics of plumes (Harris and Rose 1983; Lacasse et al. 2004). Lacasse et al. (2004) illustrated how radar can be used to locate and track volcanic clouds in near real time over Iceland and to record changes in the intensity of explosive activity. Marzano et al. (2006) also stated that ground-based weather radar could be successfully used for dynamical monitoring of volcanic ash clouds and quantitative retrieval of ash category, concentration and fall rate.

### Principles of radar

Most meteorological radars are pulse radars using a wavelength of 3–7 cm (Rinehart 1991). Electromagnetic waves at fixed preferred frequencies are transmitted from a directional antenna into the atmosphere in a rapid succession of short pulses. The short bursts of electromagnetic energy are absorbed and scattered by any meteorological targets encountered. Some of the energy is reflected back to the radar antenna and receiver. The

electromagnetic wave travels at the speed of light, and the range of the target is determined by measuring the time between transmission of the pulse and its return. Weather radars are designed to detect weather clouds, but the observer has to be able to differentiate between weather clouds and eruption plumes. Independent information such as direct sighting, seismic tremor or other data confirming the occurrence of an eruption in a particular volcano is usually the basis for identification of a volcanic plume in radar records.

### Accuracy and detection limits of radar

When considering what defines the limits and quality of radar data, we must examine the centre of the radar beam at every elevation angle and width of the beam. The centre height ($H$) of the radar beam is a function of the elevation angle $\phi$, the distance from the radar to the target ($r$) as well as the Earth's curvature (Fig. 3). Rinehart (1991) shows that $H$ can be calculated as:

$$H = \sqrt{r^2 + R'^2 + 2rR'sin(\phi)} - R' + H_0, \tag{11}$$

where $H_0$ is the radar antenna height where $R$ is the earth's radius. $R'$ is related to the atmospheric propagation and refraction. When standard conditions apply, $R'=4/3R$.

Each pulse has a beam width $\theta$ and as the distance ($r$) increases, the absolute width (e.g., meters) of the radar pulse increases according to:

$$w = r\theta \tag{12}$$

Many of the physical limitations and constraints on this observation technique are immediately apparent in Fig. 3. There is a limit to the minimum altitude that can be observed at great range due to the curvature of the Earth. A parabolic reflector in the antenna system concentrates the electromagnetic energy in a conically shaped beam that is highly directional. The absolute width of the beam increases with range, for example, a nominal 0.9 ° beam spreads to 0.8, 1.6 and 3.1 and 4.1 km at distances of 50, 100, 200 and 260 km, respectively (Eq. 12).

It is important to note that any object detected by the radar pulse is assigned the height of the centreline of the beam at distance $r$. Thus, with increasing distance from the radar, the vertical and horizontal resolution declines. For numbers relevant to Grímsvötn and the Keflavík radar, a beam width $\theta$ = 0.9° and distance of 260 km, the absolute width of the beam has reached 4.1 km.

### Altimeter records and visual inspection of plume

During the Grímsvötn eruption, visual observations were carried out from aircraft, and three plume height determinations could be made on November 2. Two measurements were made using the aircraft altimeter by flying the aircraft at the same altitude as the plume. The altimeter is set at standard atmospheric pressure, (1,013 hPa) and absolute temperature, (288 K) and the reading needs to be corrected for the actual conditions. For calibration, the corrected elevation calculated using the actual pressure is obtained through the barometric altimeter equation for constant lapse rate (e.g., Bellamy 1945):

$$h = \frac{T_0}{\beta}\left[1 - \left(\frac{P}{P_0}\right)^{\frac{R\beta}{g}}\right], \tag{13}$$

where $P$ is actual pressure, $P_0$ is standard pressure, $\beta$ is atmospheric lapse rate (here taken as the standard rate of $6.5 \cdot 10^{-3}$ km$^{-1}$), $h$ is calculated altitude above sea level (meter), $g$ is gravity (meter per square second) and $R$ is the gas constant (Joules per kilogram Kelvin). At the meteorological station at Kirkjubæjarklaustur, 75 km to the southwest of Grímsvötn (Fig. 1 for location), the atmospheric pressure was $P$=997 hPa and the temperature $T$=280 K at the time of altimeter readings (IMO data).

The third plume height estimated was done by using photos taken from aircraft at 16:19 UTC on November 2. At this time, the height is 7±1 km over the glacier 10 km north of the craters, or 8.7±1 km a.s.l., and the adjusted radar plume height is 11.5 km a.s.l.

### Radar records

The weather radar of IMO is located about 3 km from Keflavík International Airport on Reykjanes Peninsula, southwest Iceland (Fig. 1). The radar is remotely operated from IMO in Reykjavík and has been in operation since 1991, monitoring cloud cover and precipitation (Lacasse et al. 2004). Scanned images are routinely acquired every 15 min for normal weather monitoring and every 5 min during volcanic eruptions. The radar beam circles with an initial elevation angle of 0.5 °. The vertical angle is raised ten times up to an angle of 15 ° during a full scanning cycle of 2 min. The elevation angles are 0.5 °, 0.9 °, 1.3 °, 2.4 °, 3.5 °, 4.5 °, 6 °, 8 °, 10 ° and 15 ° (Hafsteinsson 2007). During the Grímsvötn eruption, MAX images were generated every 5 min by the Rainbow Software from the company AMS Gematronic (Fig. 4). A MAX image (Fig. 4) represents a two-dimensional (2D) map graphically showing the maximum reflectivity present in the vertical column over each surface point (Pohjola and Gjertsen 2006).

## Plume height and magma discharge rate

### Plume height

The plume height above sea level, recorded by the radar, is plotted in Fig. 5. The highest point observed in the MAX

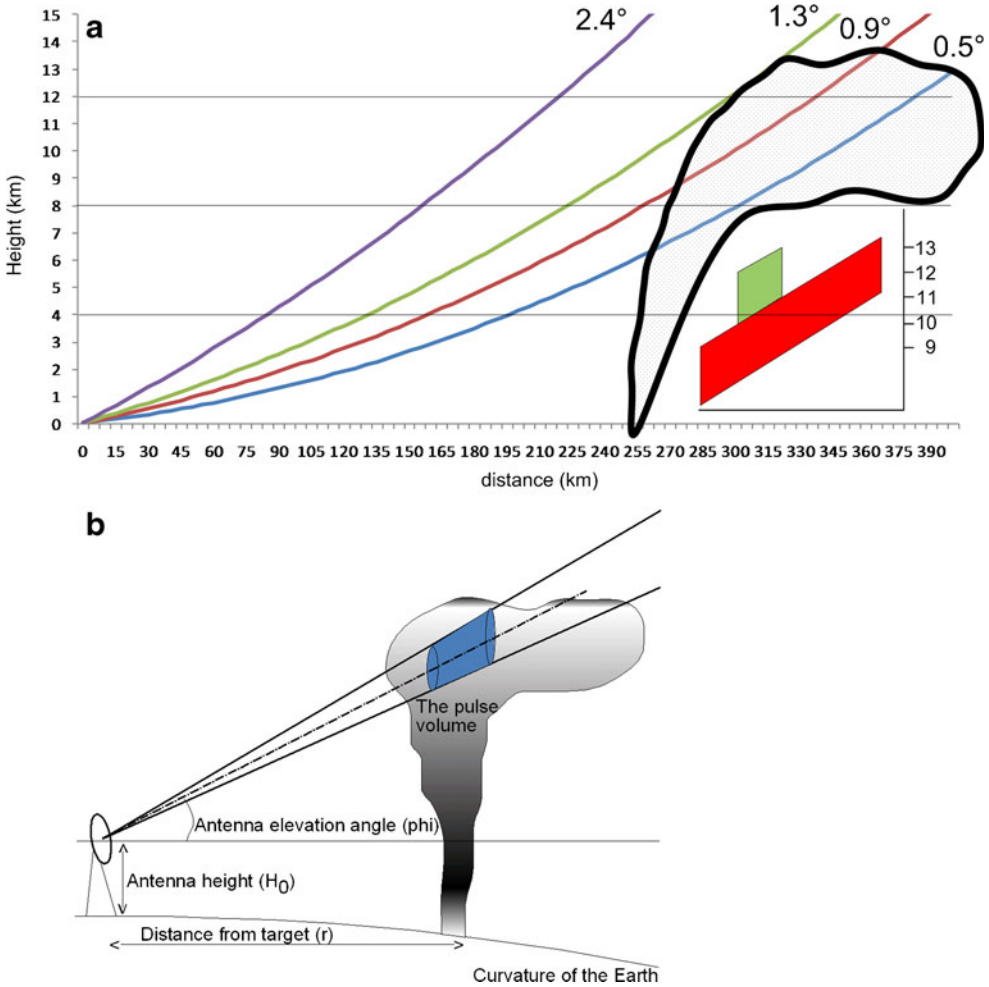


**Fig. 3** **a** Path of the radar beam at different antenna angles. The *red and green quadrants* are showing what is recorded by the radar. **b** Normal setup for weather radar. The path of the radar beam is a function of the curvature of the Earth and the elevation angle. The beam width increases with distance from the radar, and these two properties control the minimum height of the recorded object

images (Fig. 4), aquired every 5 min is used as input to the models for eruption rate (Eqs. 8–10). Height used in model calculation is relative to the eruption vent and calibrated by using the altimeter measurements and photographs (Fig. 5).

## Stepping in radar records

The increasing width of the radar beam with distance (Eq. 12) is the most important factor in limiting the accuracy of individual plume height estimates from the radar. Refraction in the atmosphere is a potential source of systematic error. The radar–volcano distance of 260 km and with the plume extending north and northeast towards the elevation determination occurs at points 260–300 km distant from the radar (and vertical absolute beam width of 4.1 km, Eq. 12). In Fig. 5a, there are several steps in the vertical altitude measurements, between 7 and 14 km a.s.l. These steps are due to the discrete nature of the measurements made at a fixed number of elevation angles defined by the scanning strategy (see "Radar records"). The time interval between two consecutive measurements every 5 min also adds to the stepwise nature of the time series. If the plume is at a height close to the detection boundary for two adjacent elevation angles, it will sometimes be registered in the lower beam and sometimes in the higher beam. This explains the jumps recorded in Fig. 5a.

## Cloud top height uncertainty

The observed difference between the measured top heights of the eruption plume by radar and the aircraft may be due to a number of reasons related to the uncertainty of the radar beam height estimate. These indicate the scanning strategy, beam width and, to some extent, the variations of vertical refractivity gradient (VRG) which will affect the accuracy of the beam height determined by Eq. 11 and assume standard propagation conditions. Table 1 gives a beam height at 260 km from the radar site for each elevation angle used in the scanning strategy. It can be seen that the difference between two consecutive vertical beams ranges from 1.8 km to 5 km up to 2.4 ° elevation which is of the same order of magnitude or larger than the observed difference between the measured top heights of the eruption plume by radar and aircraft. The 4.1 km absolute beam width at 260 km gives an

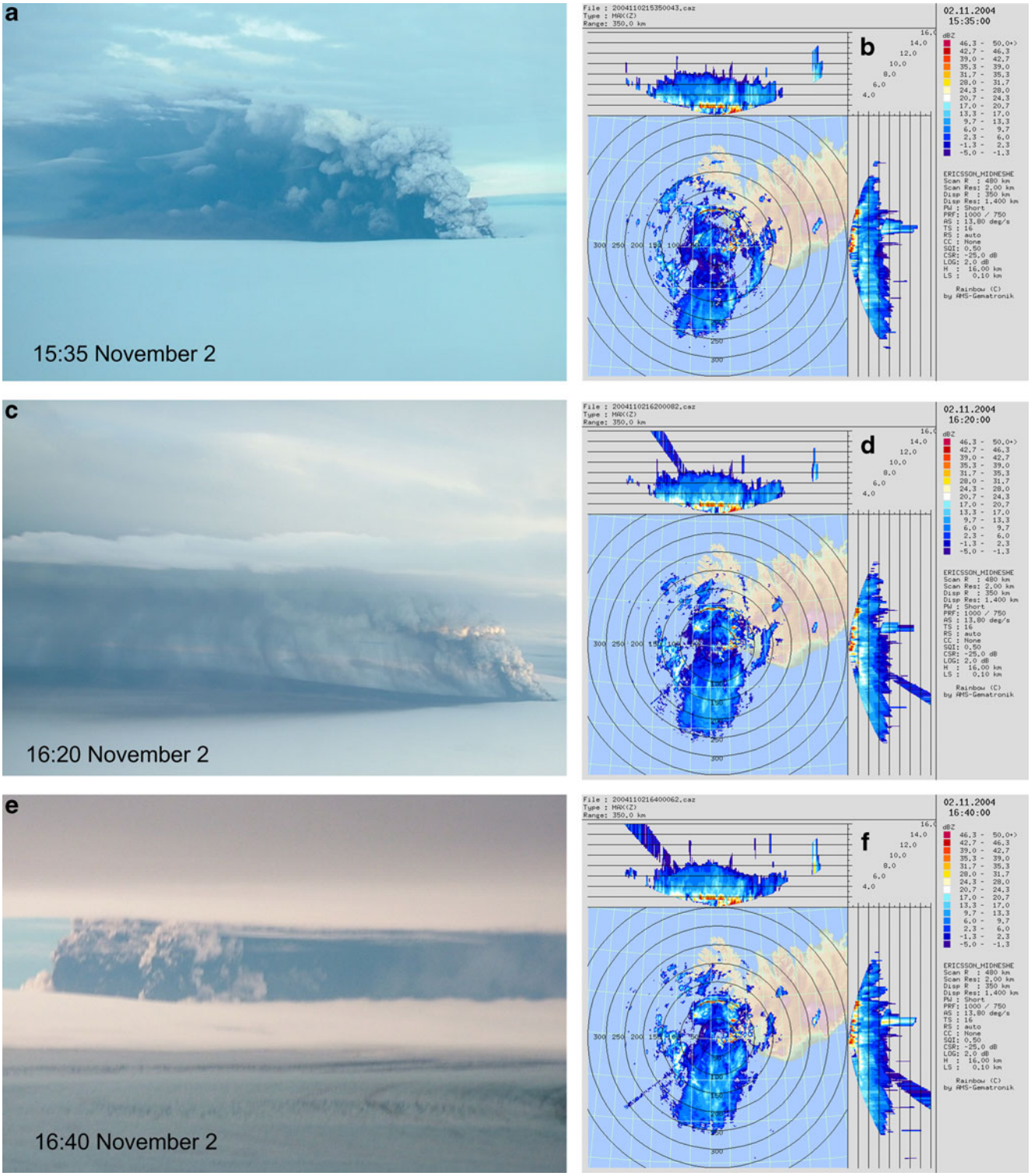


**Fig. 4** Contemporary photos (*left*) and MAX radar images (*right*), taken at 15:35 UTC (**a**–**b**), 16:20 UTC (**c**–**d**) and 16:40 UTC (**e**–**f**) on November 2. **c**–**d** The plume at 16:20 UTC is obviously lighter in colour and more transparent than at the 15:35 UTC (**a**–**b**) and 16:40 UTC (**e**–**f**). The MAX images (**b**, **d**, **f**) show recorded height and signal strength of clouds over the western part of Iceland, while the eruption plume is visible over Grímsvötn. The apparent location is displaced towards the southeast relative to the actual vents (17 km towards the east and 17 km towards the south due to misplacement in the program)

uncertainty of 2 km in the height estimate, since it cannot be determined whether the plume top is near the bottom, middle or top of the area scanned for each elevation angle. Changes in temperature, moisture and pressure with height

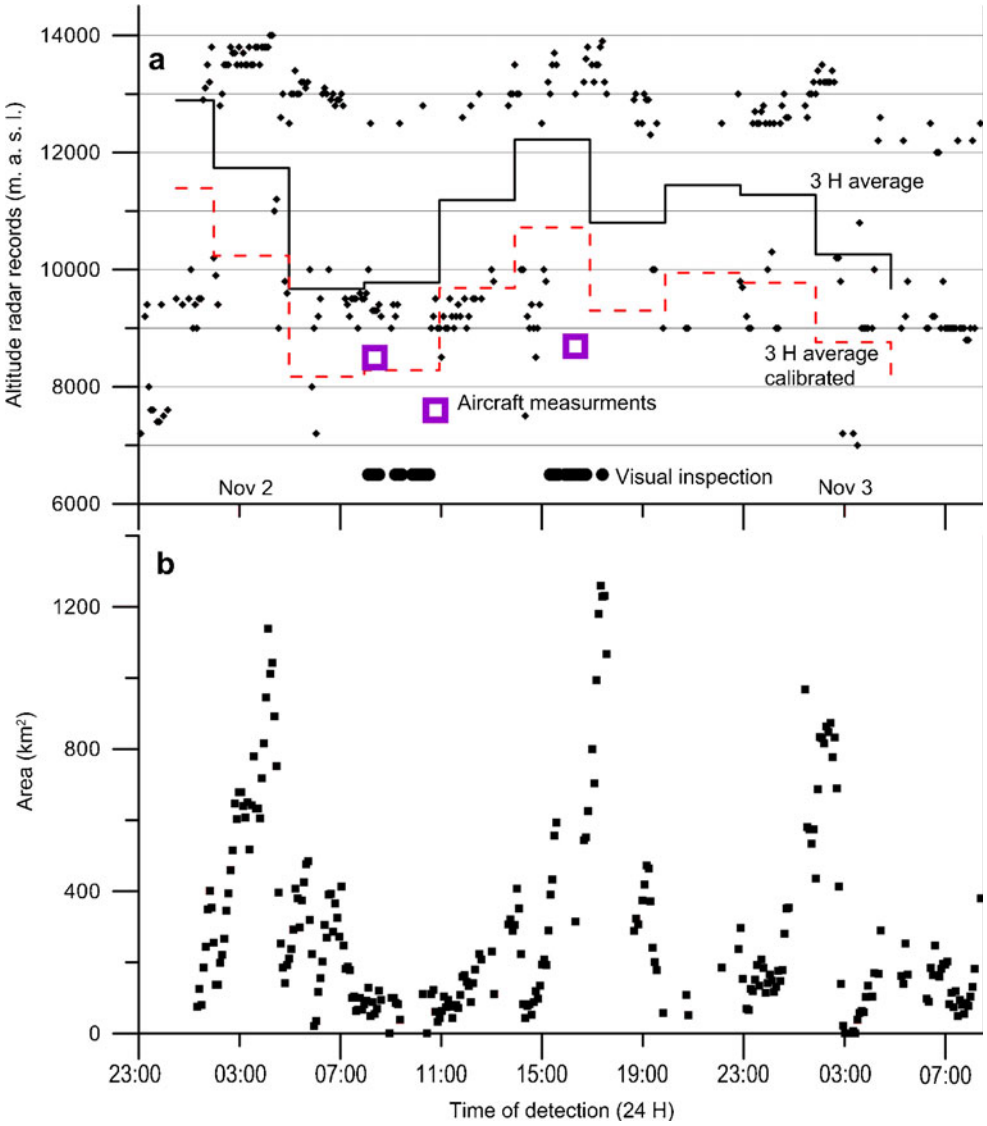


**Fig. 5** Plume height and distribution between 23:00 on November 1 and 9:00 on November 3, according to MAX images from the radar in Keflavík. **a** The maximum uncorrected height of the plume at 5-min interval (*dots*), the 3-h averages (*lines*) and the aircraft observations (*squares*). The corrected 3-h mean values are shown as a *dashed line*. **b** The area over which the plume is visible on the images. Note that possible plume dispersal below 6 km is not detected by the radar

in the atmosphere control the atmospheric density, which in turn causes variations in the speed of electromagnetic waves. These changes in speed lead to change in the propagating direction or bending of the waves. The bending of waves as they pass through the atmosphere is described with variations in the refractive index, $n$ (Rinehart 1991; Bech et al. 2003). The magnitude refractivity, $N$, is used in propagation studies (Bean and Dutton 1968):

$$N = (n-1)10^6 = \frac{77.6}{T}\left(p + \frac{4810e}{T}\right), \tag{14}$$

where $T$ is the air temperature (Kelvin), $p$ is the atmospheric pressure (hectopascals), and $e$ is the water vapour pressure (hectopascals).

The refraction of the radar beam is controlled by the VRG (Bech et al. 2003). In the $R'=4/3R$ model used in Eq. 11, VRG is $-39$ km$^{-1}$. It is the VRG in the lowest layer of the atmosphere that is especially important in estimating path and propagation effects such as sub-refraction, super-refraction and ducting.

Sub-refraction occurs where VRG$>-39$ km$^{-1}$. In this case, the beam is deflected away from the earth. In this case,

**Table 1** Centre height of the radar beam at 260 km distance from source at each elevation angle

| Elevation angle | Height at 260 km distance | Height difference |
|---|---|---|
| 0.5 | 6.24 | NA |
| 0.9 | 8.05 | 1.81 |
| 1.3 | 9.87 | 1.81 |
| 2.4 | 14.85 | 4.98 |

the radar would tend to underestimate height. When VRG<−39 $km^{-1}$, the radar beam is bent downward relative to standard refraction. This situation is called super-refraction which leads to an overestimation of plume height. In the situation of ducting, VRG is greater than −157 $km^{-1}$. Here, the beam gets trapped between boundaries in the troposphere (Rinehart 1991; Bech et al. 2003). Ducting may occur when there is a temperature inversion with increasing altitude or a sharp decrease in moisture with height. Radiosonde data from Keflavík Airport, collected twice a day only, were used to estimate the vertical gradient of refractivity in the first height kilometre (Table 2). The results do not support the idea of super–refraction, while some inversions occur in the lowermost 2 km. The data indicate, however, quite some variability which affects the quality of the estimate made by Eq. 11 using standard atmospheric conditions. Crochet (2009) studied VRG in Iceland and found very few cases of anomalous propagation over the period 2005 to 2006.

### Variation of height with time

Visual inspection from an aircraft revealed no dramatic jumps in plume height and at least in most cases, the apparent fluctuations seen on Fig. 5 are a result of small variations amplified by the radar stepping (see "Stepping in radar records"). Thus, it seems likely that the plume was more stable than Fig. 5 indicates. During the first 2–3 h of detection, the plume is gradually rising from 5 km to 8 km over vent (6.5–9.5 km over sea level, Fig. 5a). The average height after that initial period is about 8 km over the vent (~9.5 km a.s.l.). Figure 6 shows plume height versus the area covered by the plume on the MAX images. The stepping in the radar records is emphasised in the graph and support the idea of the plume jumping between two elevation angles of the radar beam. It also shows that the plume is, in most cases, recorded in the higher elevation angle when its extent was greater than 400 $km^2$.

The plume falls three times to a height of approximately 4 km relative to the vent (Fig. 7), around 05:00 UTC and 14:00 UTC on November 2 and at 03:00 UTC on November 3. These events happen when there is a sudden drop in activity at the vent, and the plume falls down below the detection limit and disappears from the radar screen. Then it grows again to similar strength as before in 30 min. This elevation (4 km) is lower than the detection limit of the radar (Eq. 7), but due to radar beam width and possible effects of super-refraction, this low elevation value may be realistic. However, due the large beam width, the actual plume height at these instances has an error margin of 2 km.

**Table 2** Vertical refractivity gradient (VRG) calculated for the first 1,000 above see level at Keflavík Airport

| Time (yyyy-mm-dd) | VRG ($km^{-1}$) |
|---|---|
| 2004-11-01 12:00 | −37.336 |
| 2004-11-01 23:00 | −40.226 |
| 2004-11-02 11:00 | −41.963 |
| 2004-11-02 23:00 | −39.413 |
| 2004-11-03 11:00 | −36.735 |
| 2004-11-03 23:00 | −31.243 |
| 2004-11-04 11:00 | −30.461 |

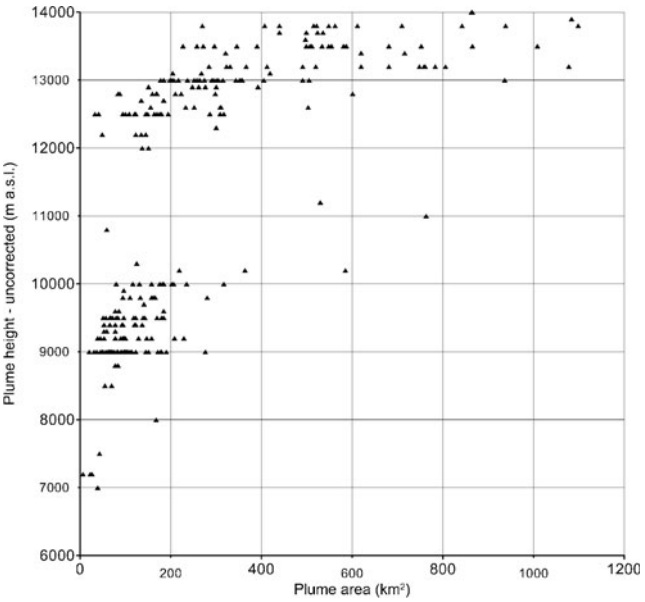


**Fig. 6** Plume height as a function of plume area as determined from the MAX images. The stepping of the plume between the two beam heights is conspicuous. Plume height tends to be higher when the area of the plume is high

## Comparison of tephra fallout with plume models

In the previous section, we have shown that the apparent large fluctuations in the plume height are a consequence of

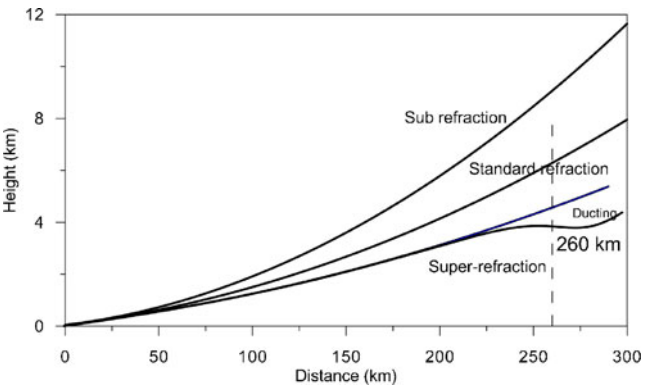


**Fig. 7** The effects of super-refraction, sub-refraction and ducting on radar-determined plume height. Here the effects of a refraction gradient of −90 $km^{-1}$ (super-refraction) are compared to standard atmosphere (−39 $km^{-1}$) considering an elevation angle of 0.5 °. The effect in this case is an overestimation of plume height by 1.6 km at a distance of 260 km. Effects of sub-refraction and ducting are also illustrated where the change in VRG is resulting in over-estimation or under-estimation of heights

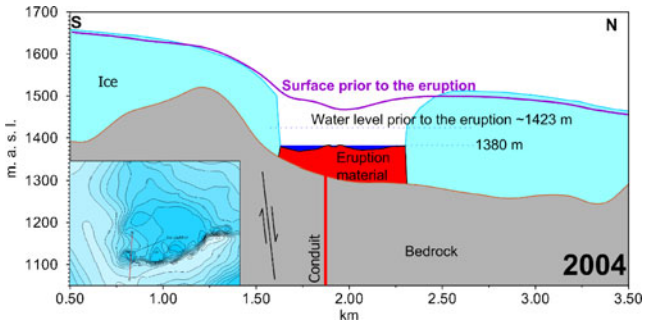


**Fig. 8** Profiles across the ice cauldron formed around the crater. Bedrock is based on radio-echo soundings from 1987 (Björnsson et al. 1992), later radio-echo surveys and the results of a seismic refraction survey carried out on the crater in 2005 (IES unpublished data)

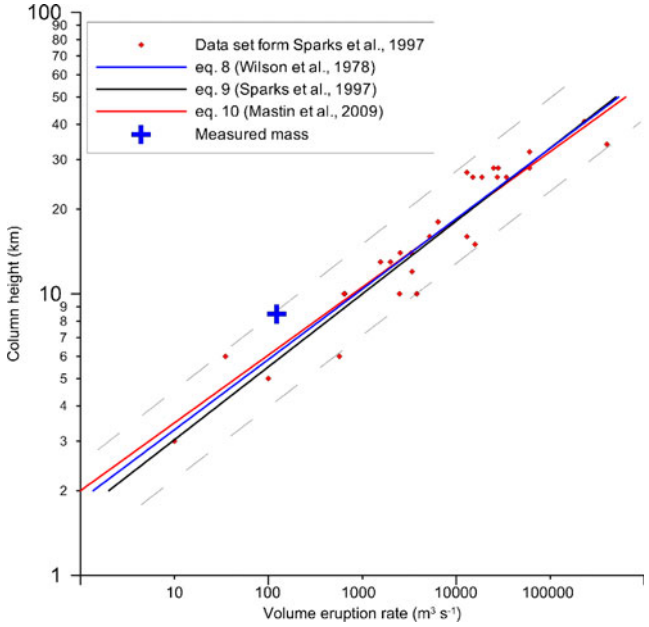


**Fig. 9** The corrected average height and average discharge of the Grímsvötn 2004 eruption compared with the empirical models of Wilson et al. (1978), Sparks et al. (1997) and Mastin et al. (2009). The scattered points are the data used to constrain the empirical models

the stepping of the radar and large beam width at large distances. When combined with the apparent occurrence of super-refraction, it is clear that the uncertainty in plume height is high. This induces a large error margin into any estimates of discharge when using plume models and distant radar data.

The part of the thermal energy of the eruption used for ice melting was not available for plume generation (Fig. 8). When comparing predicted mass from plume models with measured mass of erupted material, the mass giving away this thermal energy needs to be subtracted from the total mass. The residue, which can be called effective mass, is used here for comparison. Measurements of ice cauldron volume give $7\times10^7$ m$^3$, and using average ice density of 900 kg/m$^3$ and latent heat of fusion for ice of $3.34\times10^5$ J/kg, the energy used for ice melting was $2.2\pm0.4\times10^{16}$ J. Using magma enthalpy of $1.25\times10^6$ J/kg for the fragmented Grímsvötn tephra (Schmid et al. 2010; Gudmundsson et al. 2009), the mass of erupted material used for ice melting is $1.8\pm0.4\times10^{10}$ kg. Other thermal energy sinks are considered to be considerably smaller and are ignored here. Thus, the maximum estimate of effective mass (contributing energy to the plume) is $3.8\pm0.4\times10^{10}$ kg. This value is used in Table 3.

Table 3 shows the results of calculations using Eqs. 8–10. The radar measures height once every 5 min giving a plume height for each sampling interval. The total volume erupted over the 33 h of visible plume activity is found by summing up all the 5-min increments (integrating over time). The volume obtained from this integration is then transformed into mass of DRE using a density of 2,600 kg/m$^3$ for basaltic magmas (McBirney 1993). The numbers obtained indicate that the plume models produce total erupted mass (DRE) that is three to four times higher than the amount of the erupted material. The error margins on plume height are so wide that formally the observed values fall within the error margins of the calculated values. However, we regard the difference significant, since the aircraft determined values all fall significantly above the 5.6–6.4 km plume height (relative to vent) required for the models to fit to the observed data. Considering that none of the aircraft heights were obtained during periods of dark vigorous plume, it is improbable that the aircraft heights are biased towards high values. We, therefore, conclude that the Grímsvötn 2004 plume was significantly higher than expected from magma discharge and simple plume models.

The elevated height of the Grímsvötn 2004 plume relative to plume models based predominantly on magmatic eruptions may be related to the abundance of moisture in the plume derived from the melting ice. The effect of

**Table 3** Comparison between predicted eruption mass from plume models (Eqs. 8–10) and effective erupted mass ($M_{ef}$=3.8 · 10$^{10}$ kg, see text)

| Plume height | Eq. 8 (Wilson) | | Eq. 9 (Sparks et al. 1997) | | Eq. 10 (Mastin et al. 2010) | |
|---|---|---|---|---|---|---|
| | In kg | $M_8/M_{ef}$ | In kg | $M_9/M_{ef}$ | In kg | $M_{10}/M_{ef}$ |
| 5 min average | $1.12\cdot10^{11}$ | 300 % | $1.34\cdot10^{11}$ | 350 % | $1.03\cdot10^{11}$ | 270 % |
| 3 h average | $1.24\cdot10^{11}$ | 330 % | $1.48\cdot10^{11}$ | 390 % | $1.13\cdot10^{11}$ | 300 % |
| 8.5 km fixed | $1.16\cdot10^{11}$ | 310 % | $1.40\cdot10^{11}$ | 370 % | $1.05\cdot10^{11}$ | 280 % |

entrainment of moisture has been recognised as explaining higher plumes in moist tropical air compared to cold, dryer polar air (Sparks et al. 1997; Webley and Mastin 2009). In the case of Grímsvötn and possibly other phreatomagmatic eruptions, this effect of abundant moisture may arise from evaporation of a fraction of external water, and buoyancy acquired by the plume rises to a considerable extent from the energy released by condensation of this steam. The importance of initial buoyancy is underlined by that fact that the gas thrust region was usually very minor, with the plume being bent by the wind right from the bottom as it rose from the surface of the cauldron lake (e.g., at 16:20 UTC on 2 November, see Fig. 4).

## Summary and conclusions

Our analysis of the weather radar data on the Grímsvötn eruption in November 2004 shows the limitations and errors introduced by the large distances of over 260 km between volcano and radar station. The main factors limiting accuracy are the large width of the radar beam (e.g., 3.5 km vertically at 200 km distance) with the discrete elevation angles leading to large steps in measured plume height, deviations from standard atmospheric conditions (e.g., temperature inversions or sudden changes in lapse rate) and inability to detect low plumes due to the Earth's curvature.

Corrections obtained from aircraft-determined plume heights have been used to partly overcome the limitations of the radar. The plume of the phreatomagmatic Grímsvötn eruption in 2004, as determined by adjusted radar data was higher and carried less tephra than predicted by empirical plume models relating magma discharge with height (Fig. 9). These models are mostly based on magmatic eruptions. The eruption produced only one-third of the amount predicted from integration of plume height–magma discharge equations (Eqs. 8–10). This supports the idea that steam generated by evaporation of external water in phreatomagmatic eruptions may, in many cases, contribute significantly to the buoyancy and height of their plumes, as predicted by Koyaguchi and Woods (1996).

The distance between the radar in Keflavík and Grímsvötn is 260 km. The Eastern and Northern Volcanic Zones of Iceland have several highly active volcanoes which are even further away from the radar than Grímsvötn. Therefore, the weather radar in Keflavík is not close enough to the Eastern Volcanic Zone for monitoring volcanic plume heights with the accuracy needed. As an example, if radar is located 100 km from an eruption site, the beam width of the transmission would be 1.6 km vertically (Eq. 12) instead of the 4 km observed at Grímsvötn.

Since the eruption in Grímsvötn 2004, two explosive eruptions have occurred in Iceland: in Eyjafjallajökull in 2010 and in Grímsvötn in 2011. Both eruptions produced a significant amount of ash which was transported into the atmosphere by eruption plumes, and due to the long duration of activity in Eyjafjallajökull and northwesterly winds, air traffic in Europe was disrupted several times. IMO with the support of the International Civil Aviation Organization (ICAO) invested in a portable high-frequency dual polarisation Doppler X-band radar in 2011 for better monitoring of Icelandic volcanoes. Moreover, a second C-band radar is to be installed in East Iceland in 2012. The X-band radar was used for the Grímsvötn eruption in 2011. These improvements should lead to considerably greater accuracy of plume height in future eruptions in the eastern part of Iceland.

**Acknowledgments** The field work was done with the support of the Iceland Glaciological Society. Hálfdán Ágústsson, Katrín Auðunardóttir, Hrafnhildur Hannesdóttir and Snævarr Guðmundsson helped in the field, and Þorsteinn Jónsson gave technical support. Sverrir Guðmundsson helped with Matlab programming. Philippe Crochet is acknowledged for providing the Vertical Refractivity Gradient estimates and some useful comments to the paper. Peter Webley and an anonymous reviewer are thanked for their contribution. The project was funded by the Icelandic Research Fund and Landsvirkjun.

## References

Albino F, Pinel V, Sigmundsson F (2010) Influence of surface load variations on eruption likelihood: application to two Icelandic subglacial volcanoes, Grímsvötn and Katla. Geophys J Int 181:1510–1524. doi:10.1111/j.1365-246X.2010.04603.x

Bean B, Dutton E (1968) Radio meteorology. Dover Publications, Inc, New York

Bech J, Codina B, Lorente J, Bebbington D (2003) The sensitivity of single polarization weather radar beam blockage correction to variability in the vertical refractivity gradient. J Atmos Ocean Technol 20:845–855

Bellamy JC (1945) The use of pressure altitude and altimeter corrections in meteorology. J Meteorol 2:1–79

Björnsson H (1988) Hydrology of ice caps in volcanic regions. Rit XLV, Societas Scientarium Islandica, Reykjavík, p 139

Björnsson H, Guðmundsson MT (1993) Variations in the thermal output of the subglacial Grímsvötn caldera, Iceland. Geophys Res Lett 20:2127–2130

Björnsson H, Björnsson S, Sigurgeirsson Th (1982) Penetration of water into hot rock boundaries of magma at Grímsvötn. Nature 295:580–581

Björnsson H, Pálsson F, Guðmundsson MT (1992) Vatnajökull, Northwestern Part. 1:100 000. Bedrock Map. Landsvirkjun og Raunvísindastofnun Háskólans

Carey S, Bursik M (2000) Volcanic plumes. In: Sigurðsson H, Houghton B, Mcnutt SR, Rymer H, Stix J (eds) Encyclopedia of volcanoes. Academic Press, San Diego, pp 527–544

Crochet P (2009) Enhancing radar estimates of precipitation over complex terrain using information derived from an orographic precipitation model. J Hydrol 377:417–433

Gudmundsson MT (2005) Subglacial volcanic activity in Iceland. In: Caseldine C, Russell A, Hardardóttir J, Knudsen O (eds.) Iceland: modern processes, past environments. Elsevier, Amsterdam pp 127–151

Gudmundsson MT, Björnsson H (1991) Eruptions in Grímsvötn 1934–1991. Jökull 41:21–46

Gudmundsson MT, Sigmundsson F, Björnsson H, Högnadóttir Th (2004) The 1996 eruption at Gjálp, Vatnajökull ice cap, Iceland: efficiency of heat transfer, ice deformation and subglacial water pressure. Bull Volcanol 66:46–65

Gudmundsson MT, Zimanowski B, Jude-Eton TC, Oddsson B, Buettner R, Dellino P, Thordarson T, Larsen G (2009) Energy partitioning in the phreatomagmatic basaltic eruption of Grímsvötn in 2004. American Geophysical Union, Fall Meeting 2009, abstract #V11B-1952

Gudmundsson MT, Pedersen R, Vogfjörd K, Thorbjarnardóttir B, Jakobsdóttir S, Roberts MJ (2010) Eruptions in Eyjafjallajökull Volcano, Iceland. Eos 91:190–191

Hafsteinsson G (2007) Grímsvatnagos í Nóvember 2004: Vöktun á Veðurstofu Íslands [The eruption in Grímsvötn in November 2004: monitoring the eruption in Grímsvötn 2004 at the Icelandic Meteorological Office. In Icelandic], unpublished IMO report

Harris DM, Rose WI (1983) Estimating particle sizes, concentrations, and total mass of ash in volcanic clouds using weather radar. J Geophys Res 88:10969–10983

Höskuldsson Á, Óskarsson N, Pedersen R, Grönvold K, Vogfjörd K, Ólafsdóttir R (2007) The millennium eruption of Hekla in February 2000. Bull Volcanol 70:169–182

Jakobsson SP, Gudmundsson MT (2008) Subglacial and intraglacial volcanic formations in Iceland. Jökull 58:179–197

Jude-Eton TC, Thordarson Th, Gudmundsson MT, Oddsson B (2012) Dynamics, stratigraphy, and proximal dispersal of supraglacial tephra during the ice-confined 2004 eruption at Grímsvötn volcano, Iceland, based on field, observational and tremor data. Bulletin of Volcanology. doi:10.1007/s00445-012-0583-3

Koyaguchi T, Woods AW (1996) On the formation of eruption columns following explosive mixing of magma and surface-water. J Geophys Res 101:5561–5574

Lacasse C, Karlsdóttir S, Larsen G, Soosalu H, Rose WI, Ernst GGJ (2004) Weather radar observations of the Hekla 2000 eruption cloud, Iceland. Bull Volcanol 66:457–473

Larsen G, Gudmundsson MT, Björnsson H (1998) Eight centuries of periodic volcanism at the centre of the Iceland hotspot revealed by glacier tephrostratigraphy. Geology 26(10):943–946

Marzano FS, BarbieriS VG, Rose WI (2006) Volcanic ash cloud retrieval by ground-based microwave weather radar. IEEE Trans Geosci Remote Sens 44:3235–3246

Marzano FS, Barbieri S, Picciotti E, Karlsdóttir S (2010) Monitoring sub-glacial volcanic eruption using C-band radar imagery. IEEE Trans Geosci Remote Sens 58:403–414

Mastin LG, Guffanti M, Servranckx R, Webley P, Barsotti S, Dean K, Durant A, Ewert JW, Neri A, Rose WI, Schneider D, Siebert L, Stunder B, Swanson G, Tupper A, Volentik A, Waythomas CF (2009) A multidisciplinary effort to assign realistic source parameters to models of volcanic ash-cloud transport and dispersion during eruptions. J Volcanol Geotherm Res 186(1–2):10–21. doi:10.1016/j.jvolgeores.2009.01.008

McBirney AR (1993) Igneous petrology, 2nd edn. Jones and Bartlett Publishers, Boston

Morton BR, Taylor GI, Turner JS (1956) Turbulent gravitational convection from maintained and instantaneous sources. Proc Roy Soc Lond, Ser A, Math Phys Sci A234:1–23

Oddsson B (2007) The Grímsvötn eruption in 2004: Dispersal and total mass of tephra and comparison with plume transport models. MSc thesis, University of Iceland

Pohjola H, Gjertsen U (2006) Up to date radar based products for potential operational application. Tech. rep. Opera work package 1.6, Final report 31 October, 2006

Rinehart RE (1991) Radar for meteorologists. University of North Dakota, Grand Forks

Rose WI, Durant AJ (2009) Fine ash content of explosive eruptions. J Volcanol Geotherm Res 186:31–39. doi:10.1016/j.jvolgeores.2009.01.010

Rose WI, Kostinski AB, Kelley L (1995) Real time C band radar observations of 1992 eruption clouds from Crater Peak/Spurr Volcano, Alaska. US Geol Surv Bull 2139:19–26

Saemundsson K (1979) Outline of the geology of Iceland. Jökull 29:7–28

Schmid A, Sonder I, Seegelken R, Zimanowski B, Büttner R, Gudmundsson MT, Oddsson B (2010) Experiments on the heat discharge at the dynamic magma–water-interface. Geophys Res Lett 37:L20311. doi:10.1029/2010GL044963

Scollo S, Prestifilippo M, Spata G, D'Agostino M, Coltelli M (2009) Monitoring and forecasting Etna volcanic plumes. Nat Hazards Earth Syst Sci 9(5):1573–1585

Settle M (1978) Volcanic eruption clouds and thermal power output of explosive eruptions. J Volcanol Geotherm Res 3:309–324

Sigmundsson F, Guðmundsson MT (2004) Eldgosið í Grímsvötnum í Nóvember 2004. [The Grímsvötn eruption, November 2004. In Icelandic.]. Jökull 54:139–142

Sparks R (1986) The dimensions and dynamics of volcanic eruption columns. Bull Volcanol 48:3–15

Sparks R, Wilson L (1976) A model for the formation of ignimbrite by gravitational column collapse. J Geol Soc Lond 132:441–451

Sparks R, Bursik M, Carey S, Gilbert J, Glaze L, Sigurðsson H, Woods A (1997) Volcanic plumes. Wiley, Chichester

Stevenson JA, Lochlin S, Rae C, MacLeod A, Thordarson T (2012) Deposition in the UK of tephra from recent Icelandic eruptions. 30th Nordic Geological Winter Meeting Abstracts, 136

Thorarinsson S (1974) Vötnin stríð. Saga Skeidarárhlaupa og Grímsvatnagosa [The swift flowing rivers: the history of Grímsvötn jökulhlaups and eruptions. In Icelandic]. Menningarsjóður, Reykjavík

Thorarinsson S (1980) Langleiðir gjósku úr thremur Kötlugosum (Distant transport of tephra in three Katla eruptions). Jökull 30:65–73

Thordarson T, Larsen G (2007) Volcanism in Iceland in historical time: Volcano types, eruption styles and eruptive history. J Geodyn 43 (1):118–152

Vogfjörd K, Jakobsdóttir S, Gudmundsson GB, Roberts MJ, Ágústsson K, Arason T, Geirsson H, Karlsdóttir S, Hjaltadóttir S, Ólafsdóttir U, Thorbjarnardóttir B, Skaftadóttir T, Sturkell E, Jónasdóttir EB, Hafsteinsson G, Sveinbjörnsson H, Stefánsson R, Jónsson T (2005) Forecasting and monitoring a subglacial eruption in Iceland. Eos 86:245–252

Webley P, Mastin L (2009) Improved prediction and tracking of volcanic ash clouds. J Volcanol Geotherm Res 186(1–2):1–9. doi:10.1016/j.jvolgeores.2008.10.022

Wilson L, Sparks RSJ, Huang TC, Watkins ND (1978) The control of volcanic column heights by eruption energetics and dynamics. J Geophys Res 83:1829–1836